Journal of Materials Chemistry C

Side-chain Engineering of Self-Doped Conjugated Polyelectrolytes for Organic Electrochemical Transistors

Journal:	*Journal of Materials Chemistry C*
Manuscript ID	TC-ART-01-2023-000355.R1
Article Type:	Paper
Date Submitted by the Author:	21-Mar-2023
Complete List of Authors:	Llanes, Luana; University of California Santa Barbara, Chemistry & Biochemistry Lill, Alexander ; University of California Santa Barbara, Chemistry & Biochemistry Wan, Yangyang; California State University Northridge, Physics and Astronomy Chae, Sangmin; University of California Santa Barbara, Chemistry and Biochemistry Yi, Ahra; University of California Santa Barbara, Chemistry and Biochemistry Nguyen-Dang, Tung; University of California Santa Barbara, Center for Polymers and Organic Solids; University of California Santa Barbara, Materials Science and Engineering Kim, Hyo Jung; Pusan National University, Department of Organic Material Science and Engineering Sepunaru, Lior; University of California Santa Barbara College of Letters and Science, Chemistry Read de Alaniz, Javier; University of California Santa Barbara, Chemistry Lu, Gang; California State University Northridge, Physics and Astronomy Bazan, Guillermo; National University of Singapore Nguyen, Thuc-Quyen; University of California, Santa Barbara, Chemistry and Biochemistry

Side-chain Engineering of Self-Doped Conjugated Polyelectrolytes for Organic Electrochemical Transistors

Luana C. Llanes,[†,‡] Alexander T. Lill,[†,‡] Yangyang Wan,[⊥] Sangmin Chae,[†] Ahra Yi,[∥] Tung Dang-Nguyen,[†] Hyo Jung Kim,[∥] Lior Sepunaru,[†] Javier Read de Alaniz,[†] Gang Lu,[⊥] Guillermo C. Bazan[†§] and Thuc-Quyen Nguyen[†*]*

[‡] **The authors contributed equally to the paper**

[†]Center for Polymers and Organic Solids, Department of Chemistry and Biochemistry, University of California, Santa Barbara, Santa Barbara, CA 93106, United States of America

[§]Department of Chemistry, National University of Singapore, Singapore 117543, Singapore

[⊥]Department of Physics and Astronomy, California State University, Northridge, CA 91330, USA

[∥]Department of Organic Material Science and Engineering, School of Chemical Engineering, Pusan National University, Busan, 46241, Republic of Korea

*Corresponding author emails: quyen@chem.ucsb.edu, chmbgc@nus.edu.sg

10th Anniversary Statement

It is an honor for our groups to contribute to this special issue celebrating the 10th anniversary of Journal of Materials Chemistry C. Under the leadership of the Editor-in-Chief, Natalie Stingelin, excellent associate editors and RSC staffs, the journal has become one of the most important journals for researchers in the field of materials chemistry with the emphasis on optical, magnetic and electronic devices. We wish Journal of Materials Chemistry C continued success and look forward to reading and publishing in this journal.

ABSTRACT: A series of conjugated polyelectrolytes (CPEs) containing cyclopentadithiophene-*alt*-benzothiadiazole was synthesized. The alkyl chain length was varied from 2-5 carbons in order to investigate the effects in the optical, electrochemical and morphological properties. The CPEs are mixed conductors and can be used as the active layer in accumulation mode organic electrochemical transistors (OECTs). The transconductance, the volumetric capacitance, and the ionic and electronic conductivity are

dependent on the alkyl chain length. DFT calculations helps explain the differences in the ease of doping as a function of molecular structure.

1. Introduction

Conjugated polyelectrolytes (CPEs) are a versatile class of conjugated polymers that are defined by a molecular framework that contains an electronically delocalized backbone and pendant ionic groups. This combination of features gives CPEs the optical and charge transport properties of organic semiconductors and the processibility of polyelectrolytes. The charged side groups lead to water solubility or polymer hydration. The latter allows for the incorporation of water molecules and mobile ions into the polymer films,[1,2] thus enabling both electronic and ionic transport.[3] CPEs are therefore well suited for interfacing electronics and biology, through the development of intimate bioelectronic interfaces.[4] In addition, polarons on the polymer backbone generated by electrochemical doping can be stabilized by ionic groups in the side chains, yielding so-called "self-doped" CPEs.[5] These attributes have led to the utilization of CPEs in a variety of applications, including interfacial layers in organic photovoltaic (OPV) devices,[6,7,8,9] organic light-emitting diodes (OLEDs),[10,11,12] and organic thin-film transistors (OTFTs),[13,14] bioimaging[15], bioelectric current generation enhancement,[16] bioelectric current storage (capacitive properties),[17] antimicrobial properties,[18,19,20,21] and most recently, in organic electrochemical transistors (OECTs).[22,23,24,25]

OECTs are of relevance for bioelectronic applications. Reports demonstrate use for *in vivo* neural recording and modulation,[26,27,28,29] pH-sensing[30,31] and miniaturized biosensors for analyte detection.[32,33,34,35,36,37,38,39,40] The low operational voltage of OECTs and compatibility with aqueous environments make them useful for biological applications.[41] An OECT consists of an organic semiconductor film (active layer) between two metal electrodes (the source and the drain). On top and in direct contact with the active layer is the electrolyte, where a gate electrode is immersed.[42] An electrochemical potential can drive ions from the electrolyte into or out of the conductive layer. Injected ions modulate the doping state and, therefore, the conductivity of the active layer. Thereby, ionic signals are transduced into electronic signals.[43,44]

In this contribution, we present a structure-property relationship study on derivatives of a self-doped cyclopentadithiophene-*alt*-benzothiadiazole backbone containing pendant sulfonate groups. A series of copolymers with increasing alkyl chain distances between the conjugated backbone and the anionic groups (2-5 methylene units) were synthesized (Figure 1). OECTs were fabricated with each CPE as the active layer, and electrochemical impedance spectroscopy (EIS) was utilized to understand differences in performance. Optical, electrochemical, and morphological properties were evaluated and combined with DFT calculations to understand how alkyl chain length variation modulates the properties of OECTs.

2. Results

2.1 Synthesis and characterization

Figure 1 provides the chemical structures of the CPEs together with the synthetic approach for accessing the new structures. The synthesis of CPE-C4-Na and CPE-C3-Na has been previously reported.[45,46] For CPE-C2-Na and CPE-C5-Na the synthetic pathway begins with alkylation of commercially available cyclopentadithiophene (CPDT) followed by bromination using *N*-bromosuccinimide (NBS). For CPE-C2-Na, alkylation of CPDT with sodium 2-bromoethanesulfonate was achieved under basic conditions, followed by bromination with NBS. Synthesis of CPE-C5-Na begins by alkylation of CPDT with excess 1,5-dibromopentane under basic conditions followed by bromination with NBS. At first, alkylation of CPDT led to low yields, possibly due to intramolecular cyclization (via two successive substitutions of Br in a single 1,5-dibromopentane molecule).[47,48] An excess of 1,5-dibromopentane helped to circumvent this complication. Subsequent reaction with Na_2SO_3 in a refluxing mixture of EtOH/H_2O, aided by tetrabutylammonium iodide (TBAI) as phase-transfer reagent, afforded the anionic monomer, CPDT-C5-Na. The polymerization for all reported CPEs was achieved under Suzuki−Miyaura cross-coupling conditions. The purification procedure included precipitation of the product in acetone, filtration, and several washing steps with acetone and methanol. The resulting polymer product was purified by dialysis for three days in Millipore water, which afforded self-doped CPEs.[49,50] Lyophilization produced dark blue

solids. Detailed synthesis and characterization can be found in the Supporting Information. Counterion exchange with excess tetrabutylammonium bromide (TBABr) was performed to improve solubility in DMF and enabled gel permeation chromatography analysis.[51] The number average molecular weight was determined to be 18.1 kg mol^{-1} (CPE-C2-Na), 15.0 kg mol^{-1} (CPE-C3-Na), 11.3 kg mol^{-1} (CPE-C4-Na), 14.5 kg mol^{-1} (CPE-C5-Na).

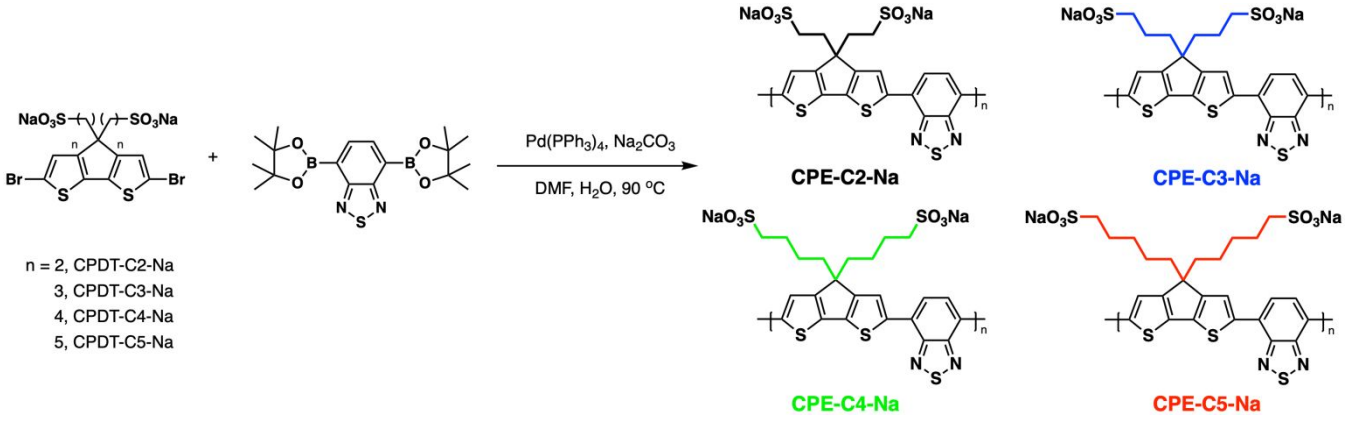

Figure 1. General pathway for Suzuki−Miyaura coupling polymerization and abbreviations used for the CPEs synthesis. The CPEs were color-coded to facilitate data visualization.

We examined the relative tendency for doping of the different CPE-CX-Na polymers by looking at the optical absorption spectroscopy. For sample preparation, CPEs were freeze-dried immediately after dialysis and used to make a 10 mg/mL solution. These were used to drop cast films onto a glass substrate or diluted to obtain the UV-Vis of aqueous solutions. Optical spectra were measured between 300 nm and 1300 nm, see Figure 2. One observes characteristic absorption peaks around 400 nm and 680 nm (λ_{max}),

previously observed for donor-acceptor copolymers containing CPDT-*alt*-BT backbones.[52,53] A first look into the absorption spectra shows a blue-shift in the neutral state absorption in CPE-C2-Na relative to the CPEs with a longer alkyl chain, see Figure 2. The broad, low-energy transition starting at 900 nm for this class of CPEs has been attributed to transitions in the doped species ($\lambda_{polaron}$).[45] The ratio between the neutral state absorbance band (~680 nm) and the polaron band should scale with the fraction of chains with polaronic states.[54,55] Comparison of the relative intensity ratios between $\lambda_{polaron}$ and λ_{max} indicates the impact of alkyl chain lengths on the doped levels, see Table S1. Going from 2 to 5 methylene units, the $\lambda_{polaron}/\lambda_{max}$ ratio increases. CPE-C2-Na exhibits a ratio of 0.36, CPE-C3-Na of 0.59, CPE-C4-Na of 0.75 and CPE-C5-Na of 0.81 (Figure 2a). UV-Vis spectroscopy measurements in thin films prepared from aqueous solutions reveal the same trend (Figure 2b). The value of $\lambda_{polaron}/\lambda_{max}$ in the film is highest for CPE-C5-Na (0.81), followed by CPE-C4-Na (0.79), CPE-C3-Na (0.64), and CPE-C2-Na (0.29). Considering that the sulfonate is thought to stabilize cationic polaronic states via Coulombic stabilization[50], it was expected that shorter alkyl chains would lead to a higher degree of doping. As mentioned above, UV-Vis spectra demonstrates an opposite effect, which will be further analyzed in the electrochemical and theoretical sections of this paper.

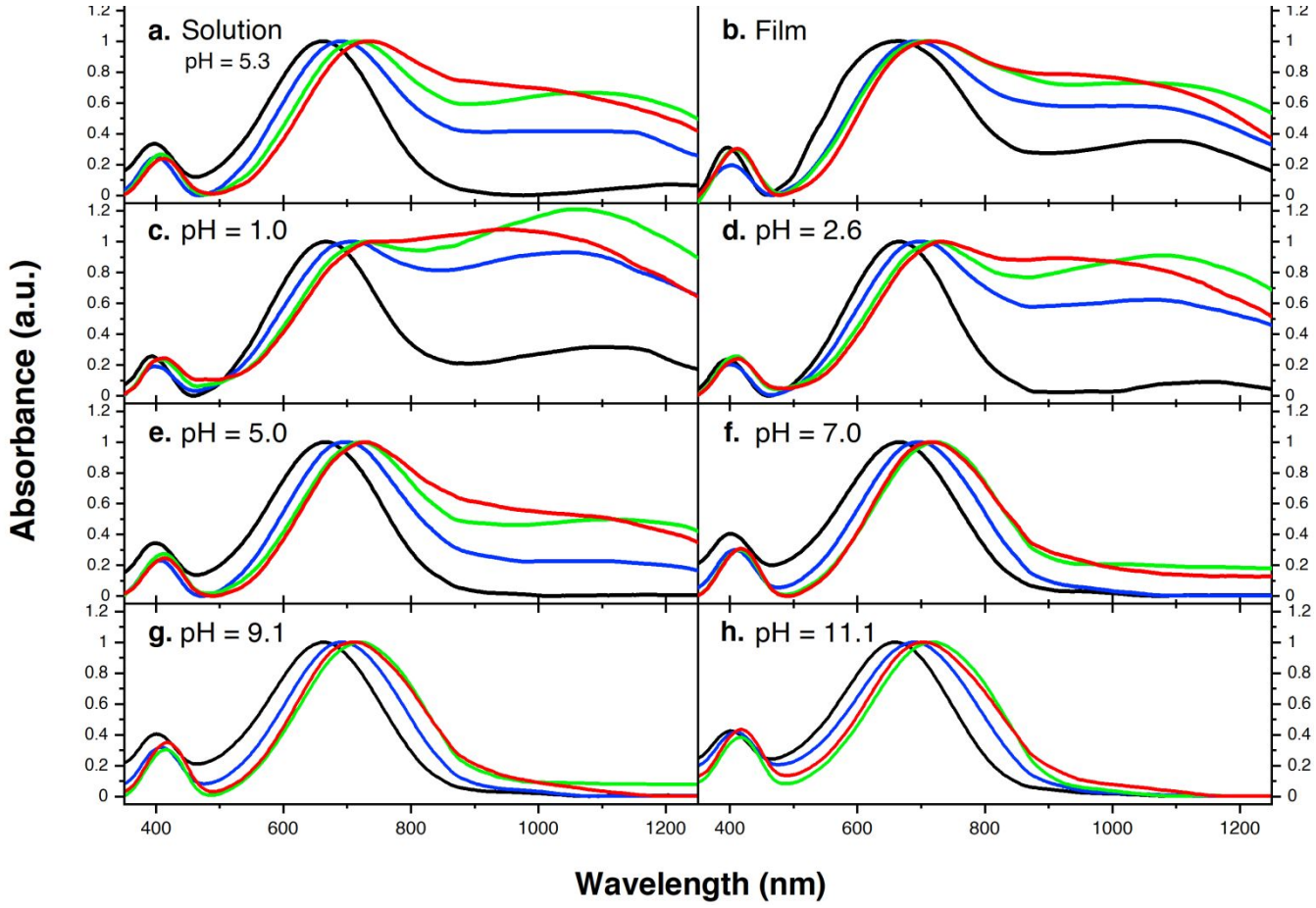

Figure 2. a) Normalized Ultraviolet-visible-near-infrared spectroscopy (UV-Vis-NIR) of aqueous CPE solutions; b) Normalized UV-Vis-NIR of CPE films deposited on ITO/glass substrates; pH dependent UV-Vis-NIR (normalized absorption) at c) pH = 1.0; d) pH = 2.6; e) pH = 5.0; f) pH = 7.0; g) pH = 9.1; h) pH = 11.1. Black: CPE-C2-Na, Blue: CPE-C3-Na, Green: CPE-C4-Na, Red: CPE-C5-Na.

From our previous study, the proposed doping mechanism for the CPEs under study consists of two steps: 1) protonation of the CPDT unit of the polymer and 2) single electron transfer from a neutral polymer chain to the protonated polymer, resulting in one polymer chain with a positive polaron and

another polymer chain with an unpaired electron.[50,56] Figure 3 exhibits the chemical equation for the doping process as described previously and CPE-C4 is selected for illustrative purposes. Since the protonation of the cyclopentadithiophene will be related to its basicity, pH dependent UV-VIS measurements were conducted (Figure 2c). Buffer solutions of pH of 1.0, 2.7, 5.0, 7.5, 9.2 and 11.3 were prepared. A solution of 3.3 μg/mL CPE in buffer was prepared and the solutions were allowed to equilibrate for 24 hours. After the UV-VIS measurement, the final pH of the solutions was determined. The intensity of the polaron absorption increased with lower pH value, indicative that the polaron concentration is higher. In a previous study with CPE-C4-K, a direct relationship between increased acidity and increase in the polaron concentration was observed via electron paramagnetic resonance studies.[57,58]

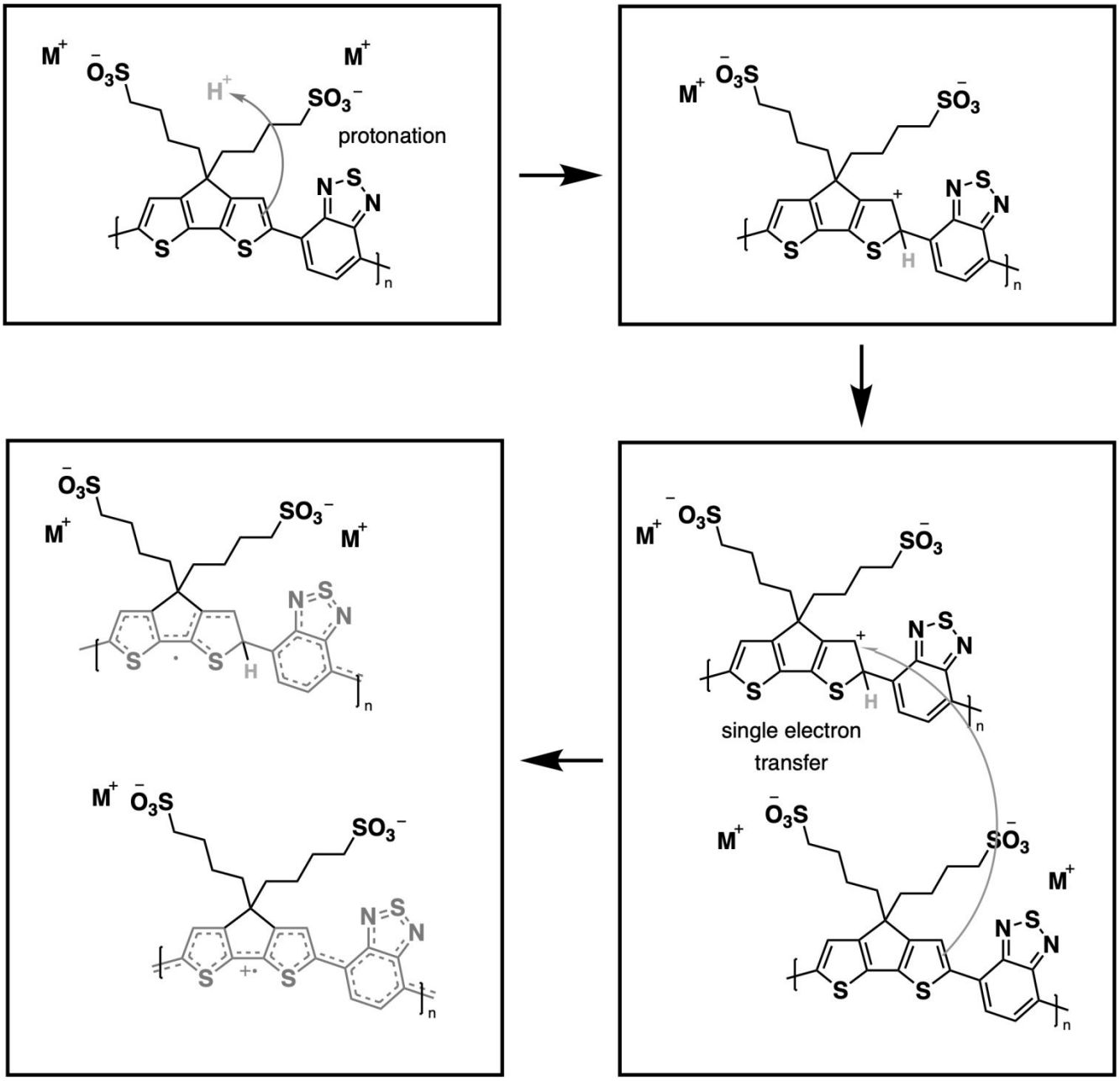

Figure 3. Schematic representation for protonic acid doping of CPE-C4 adapted from paper.[58]

Differential pulse voltammetry (DPV) was used to probe electrochemical properties as a function of chemical structure. This technique was selected over cyclic voltammetry to probe the thermodynamics of the system due to its ability to minimize background current resulting in a more sensitive measurement

of Faradaic current.[59,60] The oxidation onsets of CPE films were measured in an aqueous solution. Figure 4a provides the response of CPE-CX-Na films in the DPV experiment. The following oxidation potentials (vs. SCE) were measured E_{ox} = 0.77 V (CPE-C2-Na), E_{ox} = 0.60 V (CPE-C3-Na and CPE-C4-Na) and E_{ox} = 0.56 V (CPE-C5-Na). Non-normalized voltammograms can be found in the Supporting Information (Figure S1). DPV data for the CPE-CX-Na series suggests an electron withdrawing effect by the sulfonate group,[61] which increases E_{ox} and thereby disfavors the electron transfer step in Figure 3. To further confirm an electron withdrawing effect, DPV was carried out on the alkylated cyclopentadithiophenes monomers (CPDT-CX-Na in Figure 1). As expected, the voltammograms on monomeric units are easier to interpret (Figure 4b) and can provide more clear information on the influence of the distance between sulfonate group and backbone on the redox potential. The measured potential vs. SCE were E_{ox} = 0.76 V for CPDT-C5, increasing to E_{ox}= 0.78 V for CPDT-C4 and CPDT-C3 and E_{ox}= 0.85 V for CPDT-C2. Thus, the general trend in Figure 4b is an increase in the oxidation potential with decreasing distance between the sulfonate group and the CPDT. Non-normalized data can be found in the Supporting Information (Figure S2). The electrochemical data therefore agrees with the absorbance data. Furthermore, in Figure 2, a blueshift in the absorption was observed for CPE-C2-Na relative to the longer alkyl chain CPEs, which can be explained by an electron withdrawing effect that makes the CPDT fragment a weaker donor.

The effect of alkyl chain length on the degree of doping may also be understood by considering the effect of chain flexibility. A higher number of methylene units in the alkyl chain translates to a larger conformational space, and therefore, to a more frequent close proximity of the sulfonate group to the conjugated backbone. Such a situation would lead to a higher degree of polaron stabilization and a higher degree of doping by means of through-space coulombic stabilization.

Comparing Figure 4a and 4b one can see that, relative to the oxidation peak for monomers, the oxidation peak for the CPEs is broader and appears at lower potentials. The extended conjugation in the polymer result in the lowering of the oxidation potential compared to the monomer. With an increasing chain length of the system, the number of accessible redox states increases, which results in a superposition of redox states over a broad potential range.[62] Furthermore, the dispersity of the chains favors the superposition of redox states.[62]

Ultraviolet-photoelectron spectroscopy (UPS) was carried out (Figure 4c) on films of CPE-C2-Na, CPE-C3-Na, CPE-C4-Na, and CPE-C5-Na spin-coated atop ITO/glass substrates. The abscissa is the binding energy relative to the Fermi level of Au (E_F), which is defined by the energy of the electron before excitation relative to the vacuum level. The ionization potential (IP) onsets were obtained from the low energy region. The values for ionization potential (IP) obtained by this technique were -5.2 eV (CPE-C2-

Na), -5.2 eV (CPE-C3-Na), -5.2 eV (CPE-C4-Na), and -5.2 eV (CPE-C5-Na). The IP values were the same for all CPEs. Table 1 summarizes the data obtained for electrochemical characterization.

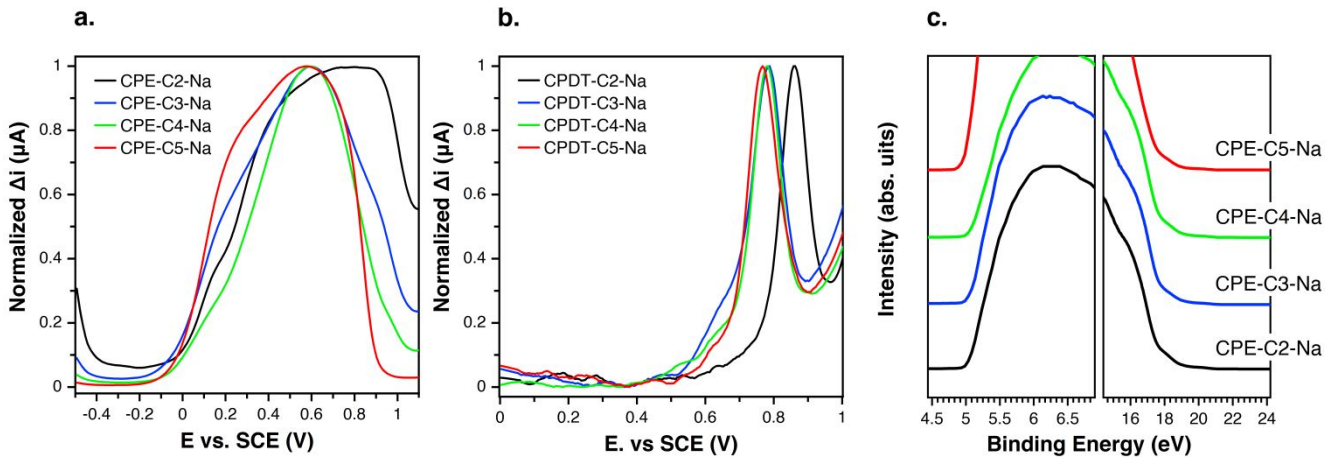

Figure 4. a) Normalized differential pulsed voltammetry on dropcasted CPE films measured in aqueous solution (0.1 M NaCl); Glassy carbon working electrode, saturated calomel as reference electrode and platinum wire as counter electrode; b) Normalized differential pulsed voltammetry on films (dropcasted) of alkylated cyclopentadithiophene derivatives measured in aqueous solution (0.1 M NaCl); c) UPS data in the high binding cut off region and highest occupied state. The ionization potential was measured by subtracting the difference between the energy of the incident photon and the width of the spectrum.

CPE	Eox (V vs. SCE)	IP (eV)
CPE-C2-Na	0.77	-5.2
CPE-C3-Na	0.6	-5.2
CPE-C4-Na	0.6	-5.2
CPE-C5-Na	0.56	-5.2

Table 1. Oxidation onset and ionization potential of CPEs.

2.2 Theoretical Studies

DFT was used to bring more insight into the doping level differences. The geometry optimizations and electronic structures calculations were performed at ωB97XD/6-31G(d)[3] level of DFT with three repeat units of CPE. The energy levels of CPE and CPE^+ (from Figure 3) are illustrated in Figure 5a and the electronic transition from the highest occupied molecular orbital (HOMO) to the lowest unoccupied molecular orbital (LUMO) corresponds to λ_{max} observed in the experiment. In CPE^+, unoccupied in-gap states are generated (polaron states) that are responsible for the redshift in absorption, i.e., the appearance of a new transition ($\lambda_{polaron}$). The intensity of $\lambda_{polaron}$ is proportional to the concentration of CPE^+ and the oscillator strength of the polaron transition. To compare the concentration of the polarons in the polymer films, the formation energies of CPE^+-CX-Na (X= 2, 3, 4, 5) were calculated following the equation from Figure 3. As summarized in Figure 5b, the formation energy of CPE^+-CX-Na (X=2, 3, 4, 5) decreases monotonously from C2 to C5. Since a larger formation energy would translate to a lower concentration of positive polarons, we find that the polaron concentration is higher when a longer alkyl chain length is included. The calculated oscillator strengths of the main peaks for CPE^+-CX-Na (X=2, 3, 4, 5) are summarized in Figure 5b, and no obvious difference can be found among the various alkyl chain lengths. Based on the above analysis, it can be concluded that the intensity of $\lambda_{polaron}$ in Figure 2a-b is attributed to the lower formation energy of CPE^+-CX-Na with longer alkyl chain lengths.

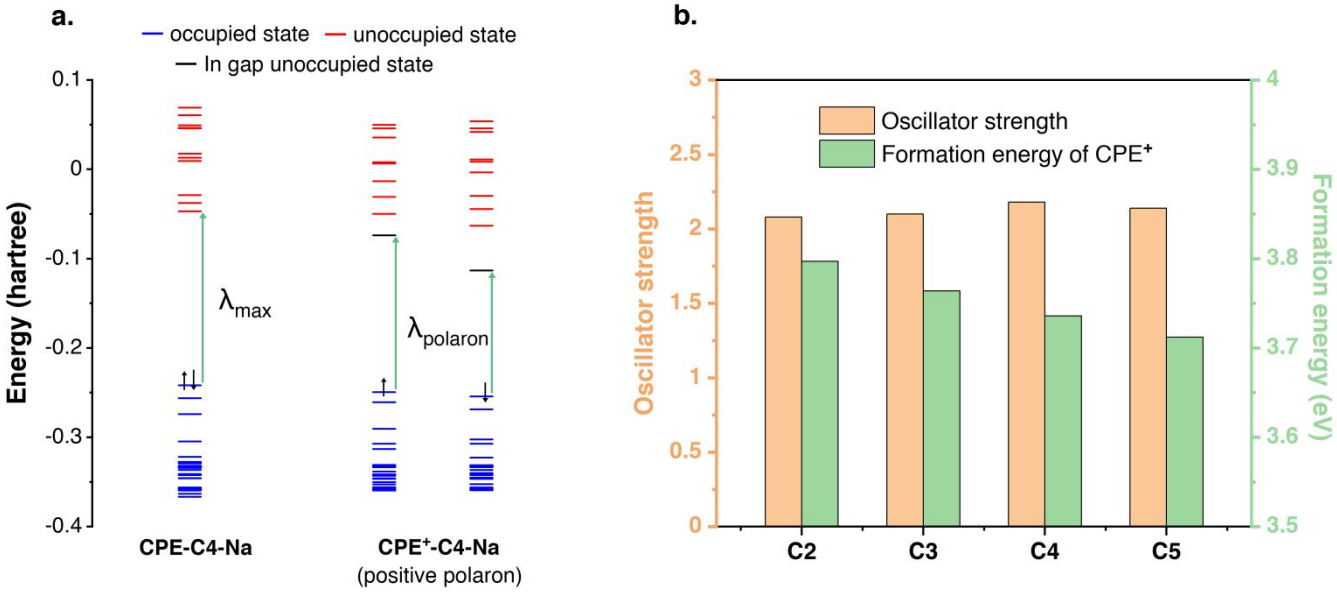

Figure 5. a) The energy levels of CPE-C4-Na and CPE$^+$-C4-Na; b) The oscillator strength and formation energy of each CPE$^+$-CX-Na (X=2, 3, 4, 5).

2.3 Morphology study of CPEs

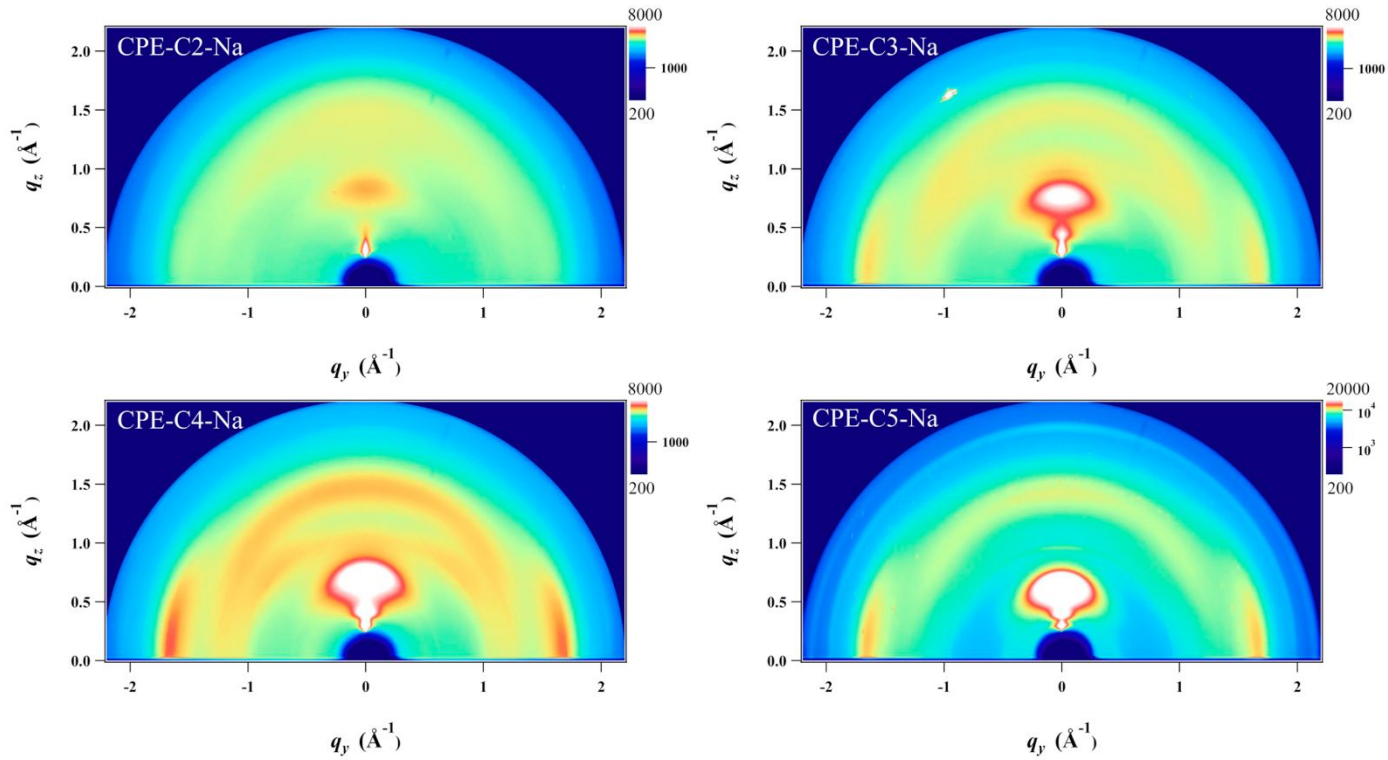

Figure 6. Grazing-incidence wide-angle X-ray scattering (GIWAXS) images of drop-casted CPE films on silicon substrates.

Grazing incidence wide-angle X-ray scattering (GIWAXS) was employed to study the structural organization of drop-cast films on Si substrates (Figure 6). A scattering peak along the q_z direction at 0.7~0.9 $Å^{-1}$ is observed, and the position of the peak scattering shifts to smaller $Å^{-1}$, which corresponds to longer lamella distance (from 0.71 nm to 0.87 nm) as increasing the alkyl side chains. Notably, the coherence length (C_L) also significantly increases (from 1.67 to 5.33) that indicates better packing order is obtained as increasing the length of alkyl side chains. All detailed analysis of the crystal is summarized in Table S2. Line cuts extracted from the 2D images of the films along with out-of-plane and in-plane directions are found on Figure S3. In addition, the scattering around 1.7 $Å^{-1}$ along the q_{xy} plane is also found which corresponds to the π-π stacking distance of 0.36 nm. No measurable difference in the π-π stacking distance is observed for the CPE films except CPE-C2-Na which possesses the longer distance (0.38 nm) which is unfavorable for charge transport. We do not observe the intense scattering peak in CPE-C2-Na, which suggests that the material is the least ordered. From the analysis, C_L of π-π stacking also increases (from 1.55 nm to 3.69 nm) with increasing the alkyl side chains.

2.4 CPEs as active layer in OECTs

Preliminary OECT characterization was performed to understand the impact of chain length variation on devices performance. Figure 7a contains the general device architecture used for our measurements. A 0.1 M solution of NaCl was used as the gate electrolyte and an Ag/AgCl pellet as the gate electrode (and pseudo-reference electrode). The CPE films were processed from water and therefore needed to be stabilized with a cross-linker, (3-glycidyloxypropyl)trimethoxysilane (GOPS), to avoid dissolution into the electrolyte medium. CPE solutions were thus prepared with GOPS as previously described.[22] A preliminary study with varying amounts of GOPS in each CPE established the minimal percentage of GOPS that resulted in stable films and the highest conductivity. The percentages of GOPs were determined to be 32 %wt for CPE-C2-Na, CPE-C3-Na and CPE-C4-Na, while 16 %wt worked best for CPE-C5-Na.[22]

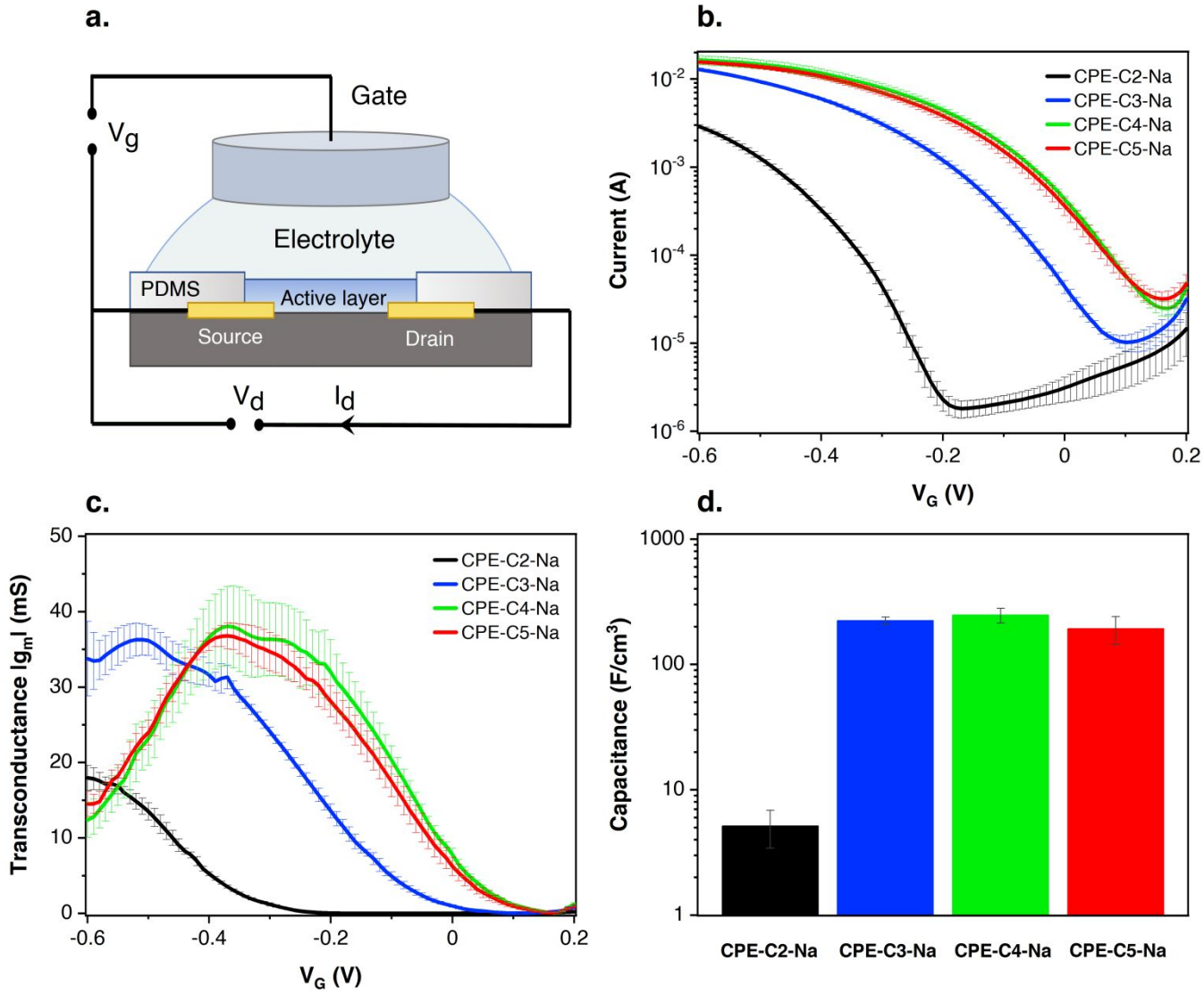

Figure 7. a) Device architecture of CPE-based OECTs; b) Transfer characteristics at $V_D = -0.6$ V of OECTs made using interdigitated contacts (W = 27 cm, L = 8 μm, d = 1.5 – 1.9 μm); c) Transconductance values at $V_D = -0.6$ V of OECTs made with interdigitated contacts. d) Volumetric capacitance measured by impedance spectroscopy.

Multiple sets of the CPE-based OECT devices were tested and the average transfer characteristics are provided in Figure 7b. Figure S4 exhibits the transfer characteristics of each run. In Figure 7b, when a

negative gate voltage is applied, Cl^- ions are introduced into the active layer. There, charges are balanced by hole injection from the source electrode, increasing the charge carrier density and therefore conductivity in the channel.[63] The negative source-drain voltage ($V_D = -0.6$ V) provides the driving force for holes migration, giving rise to the source-drain current (I_{DS}). In Figure 7b, under increasingly negative V_G, the magnitude of I_{DS} increases, characteristic of a p-type accumulation mode OECT. Accumulation-mode OECTs devices operate in the ON state and rest in the OFF state, and consume less power compared to depletion mode OECTs, which rest in the ON state. For CPE-C4-Na and CPE-C5-Na I_{DS} saturates when V_G = -0.6V. The curve for CPE-C3-Na and CPE-C2-Na still show an ascendant behavior at that voltage. Recently, OECTs based on CPE-C4-K have demonstrated the unique property of operating in the dual-mode. Under an applied negative voltage, the anion migrates and dopes CPE-C4-K, acting as accumulation mode device. In contrast, it can act in depletion mode due to the dedoping under the cation migration owing to the self-doping property.[64]

In Figure 7b, the threshold voltage (V_T) of different alkyl chain length CPEs are shifted by hundreds of millivolts. The threshold voltage is the gate voltage at which significant current starts to flow from the source to the drain[65]. The different V_T indicates a different degree of doping at specific V_G. V_T values were determined by extrapolating the corresponding $I_{DS}^{1/2}$ vs. V_G plots following a methodology reported previously (Figure S5).[66,67] V_T values of -300 mV vs. Ag/AgCl (CPE-C2-Na), -30 mV vs. Ag/AgCl (CPE-

C3-Na), 80 mV vs. Ag/AgCl (CPE-C4-Na), 70 mV vs. Ag/AgCl (CPE-C5-Na) were found. V_T of less than |0.25| V enable low voltage operation in OECT devices, which include CPEs with alkyl chain of 3, 4 and 5 methylene units.[68] We note that low threshold voltage are advantageous for sensing applications.[69,70]

The steeper the subthreshold slope, the larger the change in I_{DS} for a given change in V_G. The slope of the transfer curve is the transconductance (g_m), which indicates the signal amplification of the OECT. Under a saturation regime, g_m is given by

$$g_m = \left(W \cdot \frac{d}{L}\right) \cdot \mu \cdot C^* \cdot (V_T - V_G) \qquad (1)$$

where W is the channel width, d is the film thickness of the active layer, L is the channel length, μ is the hole mobility in the CPE channel, C^* is the volumetric capacitance of the CPE channel, V_T is a geometry-independent threshold voltage, and V_G is the applied gate voltage. Figure 7c provides the average g_m of each CPE as a function of V_G, while Figure S6 contains the transconductance of triplicate devices for each material. Peak transconductance of 36.8 ± 2 mS (CPE-C5-Na), 38.1 ± 5 mS (CPE-C4-Na), 36.3 ± 2 mS (CPE-C3-Na), and 18.0 ± 2 mS (CPE-C2-Na) were observed. CPE-C2-Na therefore exhibits poorer performance than CPEs with alkyl chain containing more than two methylene units. Table 2 summarizes the values obtained for the device characterization.

CPE	V_T (vs. Ag/AgCl)	g_m
CPE-C2-Na	-300 mV	18.0 ± 2 mS

CPE-C3-Na	-30 mV	36.3 ± 2
CPE-C4-Na	80 mV	38.1 ± 5 mS
CPE-C5-Na	70 mV	36.8 ± 2 mS

Table 2. Summary of device results.

From the GIWAXs data, there is an increase in film crystallinity for higher number of methylene units. The higher crystallinity appears to be correlated to more ordered domains and thus higher hole conductivity, resulting in OECT devices with better performance. Figure S7 of the Supporting Information shows the surface topographic images measured by atomic force microscopy (AFM) of CPE-CX-Na. The surface morphology of the CPE-CX-Na films does not change with increasing side-chain length. All films look smooth with a root mean square roughness between 0.3 and 0.4 nm.

Electrochemical capacitance quantifies the result of ion uptake of the film[71]. The doping process in our OECT devices involves Cl^- anion injection from the electrolyte into the active layer and the hole injection from the metal contact, forming sites of anion/hole pairs. A capacitor is formed between these two charge carriers originating the capacitance of the film. Equation 1 shows that g_m is proportional to C^*. Impedance spectroscopy was thus used to measure the capacitance (C) (Figure S8 in the Supporting Information), which was divided by the volume of the CPE layer (Figure 7d). Normalized to the volume, the volumetric capacitance obtained is as follows: 5.1 ± 1.7 F cm^{-3} (CPE-C2-Na), (2.2 ± 0.2) * 10^2 F cm^{-3} (CPE-C3-Na), (2.5 ± 0.3) * 10^2 F cm^{-3} (CPE-C4-Na), (1.9 ± 0.5) * 10^2 F cm^{-3} (CPE-C5-Na). CPE-C2-Na exhibits a lower volumetric capacitance while the value observed for CPE-C3-Na, CPE-C4-Na and CPE-C5-Na are similar within an error. We believe the volumetric capacitance of C2 is a factor of 50 lower due to the low

mass density from less crystallinity and low self-doping level of the material. The volumetric capacitance of the materials would decrease as the number of average charge per monomer unit decreases.[71] The UV-Vis absorption showing a much lower absorption at 1180 nm (polaron absorption) of C2 compare to C3-5,[64] indicating a significantly lower self-doping efficiency, a.k.a. lower average charge per monomer unit. We observed a similar trend with a dedoped CPE-C5-K showing two orders of magnitude smaller capacitance than a doped one.[22]

Finally, the relative ion transport of the CPEs in the dry state were evaluated using electrochemical impedance spectroscopy (EIS) (Figure S9).[72–74] A challenge associated with the measurement of CPE films is that as a conductive polymer, the high electronic conductivity would hinder measuring the ion transport. To address this and knowing that water is responsible for the self-dope efficiency of CPE-CX-Na[50], the films were annealed. CPE-CX-Na films were deposited on interdigitated contacts at 300^{o}C to drive water out of the film, thus reversibly de-doping the film without decomposing it.[50] Between two electrodes of each interdigitated contact, an AC voltage of 20mV was applied at a frequency from 10 Hz to 10 MHz. Representative Nyquist plots of each CPE material are shown in Figure S9. By fitting these plots with an equivalent circuit in Figure S10,[72] the estimated values of ion conductivity of CPE-CX-Na in the dry state were 1.96×10^{-4} S cm^{-1} (CPE-C2-Na), 1.64×10^{-4} S cm^{-1} (CPE-C3-Na), 6.34×10^{-5} S cm^{-1} (CPE-C4-Na), 3.65×10^{-5} S cm^{-1}(CPE-C5-Na). A decrease in ion conductivity is observed as the sidechain length is increased, which is attributed to the higher hydrophobic content and higher film crystallinity.

3. Conclusion

In conclusion, we have presented a systematic structure-property-relationship study on CPEs with varying side-chain lengths. Before studying this particular series of CPEs, it was hypothesized that the proximity of the polaron-stabilizing negative charge would increase the ease of doping as the side-chain length is decreased. However, the opposite trend was observed by UV-VIS. DPV of films consisting of cyclopentadithiophene derivatives as well as CPE films demonstrated a reduction in the oxidation potential with the increase in chain length. The lower oxidation potential can be interpreted with an increase in the ease of polaron formation. GIWAXS data showed an increase in crystallinity with side chain lengths which is indicative of a higher hole mobility. Finally, in DFT studies a lower formation energy was found in systems with longer alkyl chain lengths. The initial structure-property characterization suggests an electron withdrawing effect of the sulfonate group on the cyclopentadithiophene ring, making difficult the oxidation of the polymer and therefore doping. In addition, the higher flexibility of longer alkyl chain lengths can favor an approximation of the sulfonate group to the polaron, leading to a higher degree of polaron stabilization and a higher degree of doping by means of through-space coulombic stabilization. This highlights the relevance of a systematical study of conjugated polyelectrolytes to assist in the design of better materials. We concluded that shorter alkyl chain length disfavors the oxidation onset in our system and consequently reduces the doping level of the conjugated polyelectrolyte. To further explore the potential of modulating the CPE properties by alkyl chain length we performed a non-optimized OECT study. Although multiple aspects of device assembly can impact the properties, we discussed characteristics that we believe to be modulated by alkyl chain length. CPE-CX-Na, with X = 3, 4 and 5, remain viable candidates for OECT application. CPE-C2-Na shows the lowest transconductance, followed by CPE-C3-Na. CPE-C4-Na and CPE-C5-Na show similar levels of transconductance, higher than the two other materials. The OECT performance is further supported by the volumetric capacitance of each CPE.

Acknowledgement. The work was supported by the U.S. National Science Foundation (DMREF-1922042).

Author Contributions

L.C.L drafted the concept of the manuscript; A.T.L., Y.W., S.C. contributed to draft and edit the manuscript; L.C.L.: synthesized the materials, collected electrochemistry data and absorption in solution data; A.T.L.: collected absorption in films data and made and characterized the OECT devices; S.C, A. Y., H. J. K. measured and analyzed the morphological characteristics; Y.W. contributed to the theoretical section; S.C, T.D.N. contributed to OECT-related data interpretation; G.C.B., T.C.N., G.L. supervised the project, edited and revised the manuscript.

References

1 H. Jiang, P. Taranekar, J. R. Reynolds and K. S. Schanze, *Angewandte Chemie - International Edition*, 2009, **48**, 4300–4316.

2 W. Lee, J. H. Seo and H. Y. Woo, *Polymer*, 2013, **54**, 5104–5121.

3 B. D. Paulsen, K. Tybrandt, E. Stavrinidou and J. Rivnay, *Nat. Mater.*, 2020, **19**, 13–26.

4 C. Musumeci, M. Vagin, E. Zeglio, L. Ouyang, R. Gabrielsson and O. Inganäs, *Journal of Materials Chemistry C*, 2019, **7**, 2987–2993.

5 A. O. Patil, Y. Ikenoue, N. Basescu, N. Colaneri, J. Chen, F. Wudl and A. J. Heeger, *Synthetic Metals*, 1987, **20**, 151–159.

6 Z. Wu, C. Sun, S. Dong, X.-F. Jiang, S. Wu, H. Wu, H.-L. Yip, F. Huang and Y. Cao, *J. Am. Chem. Soc.*, 2016, **138**, 2004–2013.

7 J. H. Seo, A. Gutacker, Y. Sun, H. Wu, F. Huang, Y. Cao, U. Scherf, A. J. Heeger and G. C. Bazan, *J. Am. Chem. Soc.*, 2011, **133**, 8416–8419.

8 C. Sun, Z. Wu, Z. Hu, J. Xiao, W. Zhao, H.-W. Li, Q.-Y. Li, S.-W. Tsang, Y.-X. Xu, K. Zhang, H.-L. Yip, J. Hou, F. Huang and Y. Cao, *Energy Environ. Sci.*, 2017, **10**, 1784–1791.

9 Z. Hu, R. Xu, S. Dong, K. Lin, J. Liu, F. Huang and Y. Cao, *Mater. Horiz.*, 2017, **4**, 88–97.

10 C. V. Hoven, R. Yang, A. Garcia, V. Crockett, A. J. Heeger, G. C. Bazan and T.-Q. Nguyen, *Proceedings of the National Academy of Sciences*, 2008, **105**, 12730–12735.

11 J. Fang, B. H. Wallikewitz, F. Gao, G. Tu, C. Müller, G. Pace, R. H. Friend and W. T. S. Huck, *J. Am. Chem. Soc.*, 2011, **133**, 683–685.

12 X. Zhu, Y. Xie, X. Li, X. Qiao, L. Wang and G. Tu, *J. Mater. Chem.*, 2012, **22**, 15490.

13 J. H. Seo, A. Gutacker, B. Walker, S. Cho, A. Garcia, R. Yang, T.-Q. Nguyen, A. J. Heeger and G. C. Bazan, *J. Am. Chem. Soc.*, 2009, **131**, 18220–18221.

14 J. H. Seo, E. B. Namdas, A. Gutacker, A. J. Heeger and G. C. Bazan, *Adv. Funct. Mater.*, 2011, **21**, 3667–3672.

15 G. Feng, D. Ding and B. Liu, *Nanoscale*, 2012, **4**, 6150.

16 S. R. Mccuskey, Y. Su, D. Leifert, A. S. Moreland and G. C. Bazan, *Advanced Materials*, 2020, **1908178**, 1–6.

17 Y. Su, S. R. Mccuskey, D. Leifert, A. S. Moreland, L. Zhou, L. C. Llanes, R. J. Vazquez, L. Sepunaru, G. C. Bazan, S. Barbara, S. Barbara, O. Solids and S. Barbara, 1–19.

18 G. Feng, C. K. Mai, R. Zhan, G. C. Bazan and B. Liu, *Journal of Materials Chemistry B*, 2015, **3**, 7340–7346.

19 E. Zamani, T. J. Johnson, S. Chatterjee, C. Immethun, A. Sarella, R. Saha and S. K. Dishari, *ACS Appl. Mater. Interfaces*, 2020, **12**, 49346–49361.

20 E. Ji, A. Parthasarathy, T. S. Corbitt, K. S. Schanze and D. G. Whitten, *Langmuir*, 2011, **27**, 10763–10769.

21 E. Zamani, S. Chatterjee, T. Changa, C. Immethun, A. Sarella, R. Saha and S. K. Dishari, *Sci Rep*, 2019, **9**, 20411.

22 A. T. Lill, D. X. Cao, M. Schrock, J. Vollbrecht, J. Huang, T. Nguyen-Dang, V. V. Brus, B. Yurash, D. Leifert, G. C. Bazan and T. Q. Nguyen, *Advanced Materials*, 2020, **32**, 1–9.

23 M. M. Schmidt, M. ElMahmoudy, G. G. Malliaras, S. Inal and M. Thelakkat, *Macromolecular Chemistry and Physics*, 2018, **219**, 1–10.

24 E. Zeglio, M. M. Schmidt, M. Thelakkat, R. Gabrielsson, N. Solin and O. Inganäs, *Chemistry of Materials*, 2017, **29**, 4293–4300.

25 S. Inal, J. Rivnay, P. Leleux, M. Ferro, M. Ramuz, J. C. Brendel, M. M. Schmidt, M. Thelakkat and G. G. Malliaras, *Advanced Materials*, 2014, **26**, 7450–7455.

26 D. Khodagholy, T. Doublet, P. Quilichini, M. Gurfinkel, P. Leleux, A. Ghestem, E. Ismailova, T. Hervé, S. Sanaur, C. Bernard and G. G. Malliaras, *Nature Communications*, , DOI:10.1038/ncomms2573.

27 D. Khodagholy, J. N. Gelinas, T. Thesen, W. Doyle, O. Devinsky, G. G. Malliaras and G. Buzsáki, *Nat Neurosci*, 2015, **18**, 310–315.

28 J. Rivnay, H. Wang, L. Fenno, K. Deisseroth and G. G. Malliaras, *Science Advances*, , DOI:10.1126/sciadv.1601649.

29 D. Khodagholy, J. N. Gelinas, Z. Zhao, M. Yeh, M. Long, J. D. Greenlee, W. Doyle, O. Devinsky and G. Buzsáki, *Science Advances*, , DOI:10.1126/sciadv.1601027.

30 Y. J. Jo, K. Y. Kwon, Z. U. Khan, X. Crispin and T. Il Kim, *ACS Applied Materials and Interfaces*, 2018, **10**, 39083–39090.

31 G. Scheiblin, R. Coppard, R. M. Owens, P. Mailley and G. G. Malliaras, *Advanced Materials Technologies*, 2017, **2**, 1–5.

32 D. Khodagholy, V. F. Curto, K. J. Fraser, M. Gurfinkel, R. Byrne, D. Diamond, G. G. Malliaras, F. Benito-Lopez and R. M. Owens, *Journal of Materials Chemistry*, 2012, **22**, 4440–4443.

33 M. Braendlein, A. M. Pappa, M. Ferro, A. Lopresti, C. Acquaviva, E. Mamessier, G. G. Malliaras and R. M. Owens, *Advanced Materials*, , DOI:10.1002/adma.201605744.

34 E. Macchia, P. Romele, K. Manoli, M. Ghittorelli, M. Magliulo, Z. M. Kovács-Vajna, F. Torricelli and L. Torsi, *Flexible and Printed Electronics*, , DOI:10.1088/2058-8585/aad0cb.

35 A. M. Pappa, D. Ohayon, A. Giovannitti, I. P. Maria, A. Savva, I. Uguz, J. Rivnay, I. McCulloch, R. M. Owens and S. Inal, *Science Advances*, 2018, **4**, 1–8.

36 O. Parlak, S. T. Keene, A. Marais, V. F. Curto and A. Salleo, *Science Advances*, , DOI:10.1126/sciadv.aar2904.

37 J. Borges-González, C. J. Kousseff and C. B. Nielsen, *Journal of Materials Chemistry C*, 2019, **7**, 1111–1130.

38 N. Wang, A. Yang, Y. Fu, Y. Li and F. Yan, *Accounts of Chemical Research*, , DOI:10.1021/acs.accounts.8b00448.

39 C. Diacci, J. W. Lee, P. Janson, G. Dufil, G. Méhes, M. Berggren, D. T. Simon and E. Stavrinidou, *Advanced Materials Technologies*, , DOI:10.1002/admt.201900262.

40 S. Wustoni, C. Combe, D. Ohayon, M. H. Akhtar, I. McCulloch and S. Inal, *Advanced Functional Materials*, 2019, **29**, 1–10.

41 T. Someya, Z. Bao and G. G. Malliaras, *Nature*, 2016, **540**, 379–385.

42 J. Rivnay, S. Inal, A. Salleo, R. M. Owens, M. Berggren and G. G. Malliaras, *Nature Reviews Materials*, , DOI:10.1038/natrevmats.2017.86.

43 D. A. Bernards and G. G. Malliaras, *Advanced Functional Materials*, 2007, **17**, 3538–3544.

44 C. B. Nielsen, A. Giovannitti, D. T. Sbircea, E. Bandiello, M. R. Niazi, D. A. Hanifi, M. Sessolo, A. Amassian, G. G. Malliaras, J. Rivnay and I. McCulloch, *Journal of the American Chemical Society*, 2016, **138**, 10252–10259.

45 C. K. Mai, H. Zhou, Y. Zhang, Z. B. Henson, T. Q. Nguyen, A. J. Heeger and G. C. Bazan, *Angewandte Chemie - International Edition*, 2013, **52**, 12874–12878.

46 C. K. Mai, B. Russ, S. L. Fronk, N. Hu, M. B. Chan-Park, J. J. Urban, R. A. Segalman, M. L. Chabinyc and G. C. Bazan, *Energy and Environmental Science*, 2015, **8**, 2341–2346.

47 B. Liu, B. S. Gaylord, S. Wang and G. C. Bazan, *Journal of the American Chemical Society*, 2003, **125**, 6705–6714.

48 W. Lee, J. H. Seo and H. Y. Woo, *Polymer*, 2013, **54**, 5104–5121.

49 C. K. Mai, H. Zhou, Y. Zhang, Z. B. Henson, T. Q. Nguyen, A. J. Heeger and G. C. Bazan, *Angewandte Chemie - International Edition*, 2013, **52**, 12874–12878.

50 D. X. Cao, D. Leifert, V. V. Brus, M. S. Wong, H. Phan, B. Yurash, N. Koch, G. C. Bazan and T.-Q. Nguyen, *Materials Chemistry Frontiers*, , DOI:10.1039/d0qm00073f.

51 R. Yang, A. Garcia, D. Korystov, A. Mikhailovsky, G. C. Bazan and T.-Q. Nguyen, *J. Am. Chem. Soc.*, 2006, **128**, 16532–16539.

52 C. Soci, I. W. Hwang, D. Moses, Z. Zhu, D. Waller, R. Gaudiana, C. J. Brabec and A. J. Heeger, *Advanced Functional Materials*, 2007, **17**, 632–636.

53 D. Mühlbacher, M. Scharber, M. Morana, Z. Zhu, D. Waller, R. Gaudiana and C. Brabec, *Advanced Materials*, 2006, **18**, 2884–2889.

54 Z. Liang, M. J. Boland, K. Butrouna, D. R. Strachan and K. R. Graham, *J. Mater. Chem. A*, 2017, **5**, 15891–15900.

55 J. Yamamoto and Y. Furukawa, *J. Phys. Chem. B*, 2015, **119**, 4788–4794.

56 C. C. Han and R. L. Elsenbaumer, *Synthetic Metals*, 1989, **30**, 123–131.

57 D. Tsokkou, L. Peterhans, D. X. Cao, C. Mai, G. C. Bazan, T. Nguyen and N. Banerji, *Adv. Funct. Mater.*, 2020, **30**, 1906148.

58 P. S. Marqués, G. Londi, B. Yurash, T.-Q. Nguyen, S. Barlow, S. R. Marder and D. Beljonne, *Chem. Sci.*, 2021, **12**, 7012–7022.

59 Venton, B. Jill and DiScenza, Dana J., in *Electrochemistry for Bioanalysis*, Elsevier, 2020.

60 S. Rasmussen, in *Encyclopedia of Polymeric Nanomaterials*, eds. S. Kobayashi and K. Müllen, Springer Berlin Heidelberg, Berlin, Heidelberg, 2013, pp. 1–13.

61 Z. J. Zhang and X. Y. Chen, *Electrochimica Acta*, 2018, **282**, 563–574.

62 J. Heinze, B. A. Frontana-Uribe and S. Ludwigs, *Chemical Reviews*, 2010, **110**, 4724–4771.

63 R. Colucci, H. F. de P. Barbosa, F. Günther, P. Cavassin and G. C. Faria, *Flex. Print. Electron.*, 2020, **5**, 013001.

64 T. Nguyen-Dang, S. Chae, J. Chatsirisupachai, H. Wakidi, V. Promarak, Y. Visell and T. Nguyen, *Advanced Materials*, 2022, **34**, 2200274.

65 Y. Taur, in *Encyclopedia of Materials: Science and Technology*, Elsevier, 2001, pp. 9430–9444.

66 A. Savva, R. Hallani, C. Cendra, J. Surgailis, T. C. Hidalgo, S. Wustoni, R. Sheelamanthula, X. Chen, M. Kirkus, A. Giovannitti, A. Salleo, I. McCulloch and S. Inal, *Adv. Funct. Mater.*, 2020, **30**, 1907657.

67 N. Wang, L. Xie, H. Ling, V. Piradi, L. Li, X. Wang, X. Zhu and F. Yan, *J. Mater. Chem. C*, 2021, **9**, 4260–4266.

68 C.-Y. Yang, D. Tu, T.-P. Ruoko, J. Y. Gerasimov, H.-Y. Wu, P. C. Harikesh, R. Kroon, C. Müller, M. Berggren and S. Fabiano, *arXiv:2106.07438 [cond-mat, physics:physics]*.

69 J. Rivnay, P. Leleux, M. Sessolo, D. Khodagholy, T. Hervé, M. Fiocchi and G. G. Malliaras, *Adv. Mater.*, 2013, **25**, 7010–7014.

70 S. E. Doris, A. Pierre and R. A. Street, *Adv. Mater.*, 2018, **30**, 1706757.

71 C. M. Proctor, J. Rivnay and G. G. Malliaras, *J. Polym. Sci. Part B: Polym. Phys.*, 2016, **54**, 1433–1436.

72 B. X. Dong, C. Nowak, J. W. Onorato, J. Strzalka, F. A. Escobedo, C. K. Luscombe, P. F. Nealey and S. N. Patel, *Chem. Mater.*, 2019, **31**, 1418–1429.

73 B. X. Dong, Z. Liu, M. Misra, J. Strzalka, J. Niklas, O. G. Poluektov, F. A. Escobedo, C. K. Ober, P. F. Nealey and S. N. Patel, *ACS Nano*, 2019, **13**, 7665–7675.

74 B. X. Dong, P. Bennington, Y. Kambe, D. Sharon, M. Dolejsi, J. Strzalka, V. F. Burnett, P. F. Nealey and S. N. Patel, *Mol. Syst. Des. Eng.*, 2019, **4**, 597–608.

75 B. X. Dong, C. Nowak, J. W. Onorato, J. Strzalka, F. A. Escobedo, C. K. Luscombe, P. F. Nealey and S. N. Patel, *Chem. Mater.*, 2019, **31**, 1418–1429.